Geo-Mar Lett
DOI 10.1007/s00367-010-0206-y

ORIGINAL

Acoustic density measurements of consolidating cohesive sediment beds by means of a non-intrusive "Micro-Chirp" acoustic system

Ho Kyung Ha · Jerome P.-Y. Maa · Charles W. Holland

Received: 9 September 2009 / Accepted: 9 March 2010

Abstract A non-intrusive "Micro-Chirp" acoustic system and a signal-processing protocol have been developed to estimate the bulk density of consolidating cohesive sediment beds. Using high-frequency (300–700 kHz) Chirp acoustic waves, laboratory measurements were conducted with clay–water mixtures. Because acoustic echo strength is proportional to variations in acoustic impedance, and the speed of sound in the clay bed hardly changed during consolidation, the bulk density could be successfully estimated without disturbing the sediment bed. Based on acoustic signal analysis, this study demonstrates that the reflection coefficient and bulk density at the water–sediment interface increase with consolidation time, and that a single speed of sound value can be used for practical bulk density estimation in muddy environments.

Introduction

Cohesive sediment deposits are ubiquitously found along many coasts and estuaries (Flemming 2002; Partheniades 2006). Such sediments generally exhibit the strongest gradients in physical properties near the water–sediment interface (Mehta and Dyer 1990; Winterwerp and van Kesteren 2004; Holland et al. 2005). These gradients result from repeated bed formation and destruction caused by complex near-bed processes (e.g., erosion, deposition, consolidation, and bioturbation). Understanding the properties (e.g., bulk density and erosion threshold) of the uppermost layer (≈0.1 m) therefore can provide important information on sedimentary history and mechanical sediment behavior.

A number of studies have addressed the characteristics of the top layer of consolidating and/or consolidated beds (e.g., Hawley 1981; Torfs et al. 1996; Sills 1998; Lintern et al. 2002; Winterwerp and van Kesteren 2004). Nonetheless, there are few reliable methods to adequately measure the bulk density of this layer, because most current approaches are of the intrusive type, and commonly severely disturb the target layer (e.g., Hamilton 1971; Briggs and Richardson 1996; Maa et al. 1997; Seifert et al. 2008; Stark and Wever 2009). Direct coring is therefore still considered as the standard against which to compare other methods requiring elaborate calibrations for estimations of bulk density. Coring, however, is a time- and labor-intensive procedure, and cannot provide the high spatial and temporal resolutions required for most purposes.

Alternative techniques include (1) nuclear-ray (e.g., γ- and X-ray) attenuation, (2) attenuation of natural radioactivity, (3) electrical impedance change, (4) tuning fork, and (5) acoustic wave attenuation. The principle of a nuclear device is based on the fact that sediments absorb more nuclear radiation as the bulk density increases (Hirst et al. 1975; Been and Sills 1981; Sills 1997, 1998; de Groot et al. 2009). Thus, the attenuation of nuclear radiation passing through a sediment layer can be used as a proxy for estimating the bulk density. In addition, the relationship between the concentration of natural radioactive isotope and sediment properties can be used to determine the sediment composition and bulk density (Jacob

H. K. Ha (✉)
Korea Polar Research Institute, KORDI,
Incheon 406-840, South Korea
e-mail: hokyung.ha@gmail.com

J. P.-Y. Maa
Department of Physical Sciences,
Virginia Institute of Marine Science, School of Marine Science,
College of William and Mary,
Gloucester Point, VA 23062, USA

C. W. Holland
Applied Research Laboratory, Pennsylvania State University,
State College, PA 16804, USA

Published online: 24 March 2010

et al. 2009). The use of a nuclear probe, however, requires licenses and training for safe operation, and any loss in the field may generate a serious contamination problem. The electrical method is based on the principle that the sediment itself is a poor conductor in comparison to water, and that the overall conductivity depends mainly on the pore water content and its salinity (Libicki and Bedford 1989; Dowling 1990). It has been suggested, however, that this method is not suitable in brackish environments where the salinity varies frequently (Winterwerp and van Kesteren 2004). More recently, a tuning fork method has become commercially available for in-situ density measurements (Fontein and van der Wal 2006). The application of this instrument, however, is limited to low-density fluid mud, so that integration with other methods (e.g., acoustic) would be required to extend the sensing range to underlying, higher-density sediment layers.

The drawbacks of both the intrusive and non-intrusive techniques mentioned above emphasize the need for a less complicated, non-intrusive method. One such alternative could be the measurement of physical sediment properties by acoustic remote sensing (Libicki and Bedford 1989; Verbeek and Cornelisse 1995; Maa et al. 1997; Holland et al. 2005; Kaya et al. 2008). Since the acoustic echo strength is proportional to the acoustic impedance (i.e., the product of the speed of sound and density), bulk density can be calculated by the analysis of acoustic signals returned from the sediment bed (Maa and Lee 2002; Holland et al. 2005; Kaya et al. 2008). Conventional acoustic sub-bottom profilers have been used for decades to measure the geo-acoustic properties of subsurface sediments. However, the vertical resolution of such instruments is generally too low to be of any use for the identification of changes in bulk density within the near-surface sediment layer. Nevertheless, in recent years, promising advances have been made by the development of parametric echo-sounders (e.g., Schrottke et al. 2006).

In the present study, we have explored the possibility of estimating the bulk density and consolidation state of muddy sediments using high-frequency (300–700 kHz) Chirp acoustic waves. The main objectives were (1) to develop a non-intrusive acoustic system and a data-processing protocol for measuring the bulk density without destroying the sediment fabric, and (2) to understand the acoustic response to a progressively consolidating clay bed.

Materials and methods

Experimental apparatus

Consolidation experiments were conducted in a cylindrical consolidation tank (diameter: 0.75 m; height: 1.5 m). An immersion-type transducer (Olympus Inc., V389-SU) served as the transmitter, and another (Olympus Inc., V301-SU) served as the receiver. The two transducers were installed together spaced at a horizontal distance of 0.05 m. An arbitrary function generator (AFG; Gage Applied, CG1100) generated the Chirp acoustic waves, which were fed into a 25-watt power amplifier (Amplifier Research, 25A250A) for delivering the required power to excite the transmitter (Fig. 1). Since the acoustic return signal was weak, a 60-dB linear signal conditioner (Nsite LLC, SC60) was used to boost the signal up to a workable range between 0 and 4 V. For the purpose of producing comparable data, the gain settings in both the power amplifier and signal conditioner were maintained constant for all measurements. With a sampling rate of 10 MHz, the conditioned signals were digitized by a 12-bit analog-to-digital converter (ADC; Gage Applied, CS1250). By using the transistor-transistor logic (TTL) trigger signal, the generation of the source signal and the digitization of the return signal were triggered simultaneously. A triggering device incorporating a 555-timer circuit synchronized these processes at 50 Hz. For each dataset, successive 100 repeated measurements were ensemble-averaged to reduce noise. At the beginning of the echo signal digitization, there was a short time period (0–150 μs) in which data were severely contaminated by the side lobes of the source transducer, and the large relic vibration of the transducer after emitting acoustic waves. Thus, they were purposely replaced by 0 V within that period.

Chirp source signal

As a source signal, Chirp acoustic waves were employed to excite the transmitting transducer. This kind of signal,

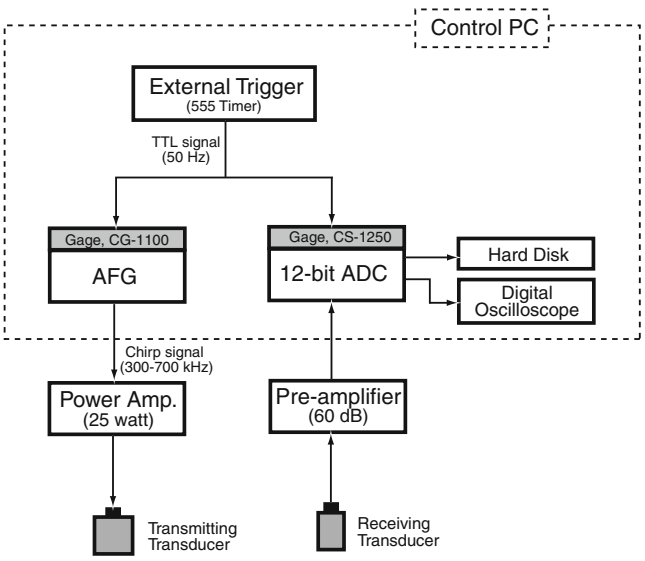

Fig. 1 Block diagram of the Micro-Chirp acoustic system developed in this study. The external trigger source, the arbitrary function generator (*AFG*), and the analog-to-digital converter (*ADC*) are all integrated into the control PC

comprising a frequency-modulated (FM) and an amplitude-modulated (AM) wave form (Fig. 2; Maa and Lee 2002), has been widely used in sub-bottom profiling systems (e.g., LeBlanc et al. 1992) to improve signal-to-noise ratios (SNRs) in signal processing. After the predetermined signal duration (≈37 μs), the signal remains zero until the next triggering event occurs. Details of the advantages gained by using the Chirp source signal, rather than traditional pulse-type signals, have been presented in Maa and Lee (2002).

The high-frequency (300–700 kHz) Chirp signal array was generated by

$$y(i) = \sin\left(\frac{i\pi}{n}\right)\sin\left(\frac{2(i-1)\pi}{T}\right) \quad (1)$$

where T is the wave period, varying as T=260–0.03 (i–1), with i=1 to n, and n=3,000. The first sine function plays a role in modulating the wave amplitude, while the second one is for modulating the wave frequency. Discrete data generated by Eq. 1 were loaded to the AFG through its built-in wave form editor. At a digital-to-analog conversion rate of 80 MHz, Chirp acoustic waves were generated with a central frequency of approx. 500 kHz (Fig. 2). The frequencies at the left and the right wing of the generated waves were about 300 and 700 kHz, respectively. It is noted that the wave form in Fig. 2 is somewhat different from the original Chirp specification (LeBlanc et al. 1992), which used a Gaussian distribution function to modulate the wave amplitude. Instead, we used a sinusoidal wave form, because Maa and Lee (2002) confirmed that it is as good as the Gaussian function in terms of signal modulation and SNR control. The integrated system developed in this study is named the "Micro-Chirp" system, after the Chirp acoustic waves.

Experimental procedures

A commercially available kaolinite clay (d_{50}≈1 μm) was used in this experiment. For the sediment preparation, the dry kaolinite was mixed with tap water for about 30 days to reach a fully water-saturated condition. The kaolinite slurry was further diluted with tap water, and mixed by running three submersible pumps with different vent directions to generate a homogeneous mixture in the tank. The initial concentration was approx. 45 g l^{-1}, and the initial height of the water column was 1.40 m. After mixing for 24 h, all pumps were stopped and removed from the tank to enable the suspended sediments to settle and consolidate.

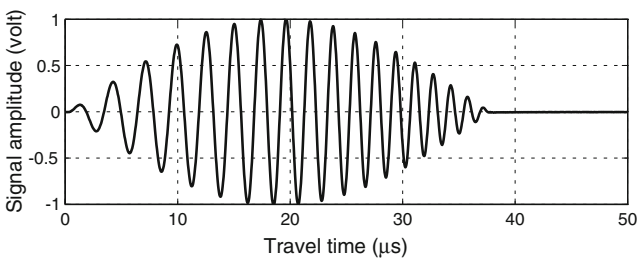

Fig. 2 Transmitted Chirp acoustic waves. The central frequency is about 500 kHz, and the frequency range is 300–700 kHz

The two downward-looking transducers were installed at 0.1 m below the water surface. Care was taken to avoid air bubbles beneath the transducers, because these can significantly affect the acoustic scattering response (Mole et al. 1972; Skaropoulos et al. 2003). Acoustic return signals were sequentially recorded at elapsed time intervals of 5, 24, 216, 338, 484, and 1,034 h. Through the translucent sidewall of the tank, the changing height of the water–sediment interface above the tank bottom was recorded over the entire experimental period. Using a syringe, clay–water mixtures were extracted through several sampling ports (0.1, 0.2, 0.4, 0.6, 0.8, 1.0, 1.15, and 1.3 m above the tank bottom) in the sidewall. The withdrawn samples were filtered through 0.7-μm glass-fiber filters when the concentration of a sample was expected to be low (ca. <0.5 g l^{-1}). When a sample was collected below the water–sediment interface at a relatively high sediment concentration, a pre-weighed aluminum pan was used to hold the sample. The residues on the filters (or the samples on the aluminum pan) were oven dried at 103–105°C for 24 h, cooled in a desiccator for 2 h, and then weighed to determine dry sediment mass, M_s. With the given volumes of the sediment samples, V_t, and assuming a solid sediment density of ρ_s=2.65 g cm^{-3}, the bulk density (ρ_b) was calculated from the relation

$$\rho_b = \frac{M_s}{V_t} + \rho_w(1-\varphi_s) \quad (2)$$

where $\varphi_s = M_s/V_t/\rho_s$ is the sediment volume fraction in the unit volume of sample, and ρ_w is the water density.

Data processing

The digital signal processing (Fig. 3) mostly utilized functions available in the Matlab® signal-processing toolbox. The first step was signal normalization. Because each measurement has echo signal strengths acquired at different ranges, the beam spreading and sound attenuation along the propagation path in the water column must be compensated. The received signal pressure (P) at the transducer can be expressed as

$$P(z,\,t) = R(\theta,z,t)\frac{P_0\sqrt{B(\theta)}}{2z}\,e^{-2\alpha z} \quad (3)$$

where P is proportional to the measured signal amplitude in volt, and P_0 is the source level (reference to 1 m), R the reflection coefficient, B the beam pattern factor (a Gaussian distribution with −3 dB beam width at ±2.3°), θ the beam angle, α the sound attenuation coefficient, z the height above the bed, and t the duration for consolidation.

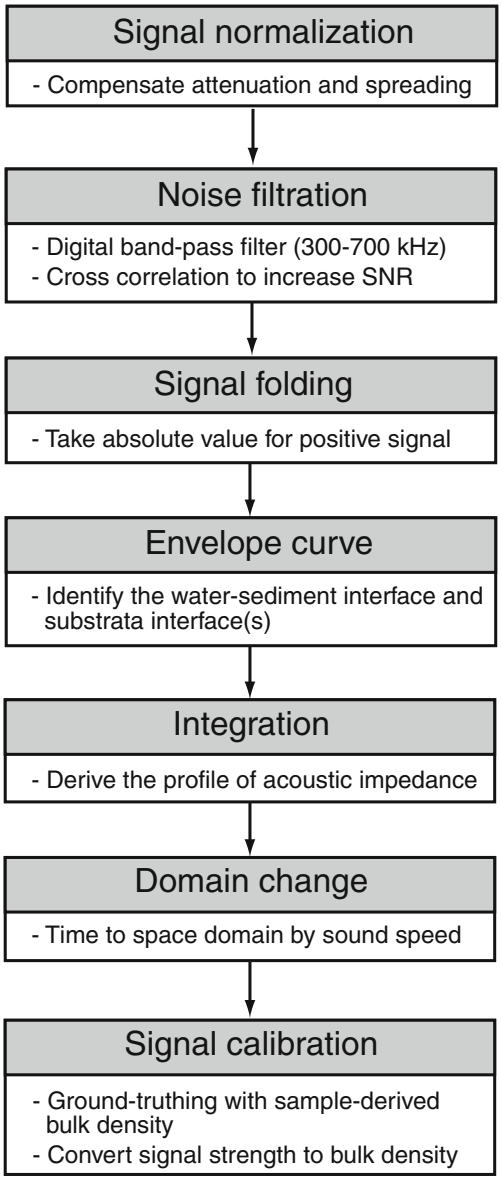

Fig. 3 Flow chart for digital signal processing. *SNR* Signal-to-noise ratio

The second step was the noise filtration to improve the SNR. In order to filter out undesirable noise embedded in the return waves, a digital band-pass filter was implemented to remove signals from the given bandwidth (i.e., 300–700 kHz). As a third and more powerful de-noising technique, we used cross-correlation to significantly increase the SNR, and to determine the existence and location of any interface caused by the difference in acoustic impedance. Mathematically, the cross-correlation of two signals, $f(t)$ and $g(t)$, is defined by

$$r(\tau) = \int f(t)g(t+\tau)\mathrm{d}t \tag{4}$$

where $f(t)$ is the raw return signal, $g(t)$ the source signal, and τ has the effect of shifting $g(t)$ forward in time relative to $f(t)$ (Stearns 2003). The correlation value, $r(\tau)$, is high if the source is similar to the return signal—that is, it represents the degree of confidence in detecting the true return signal. When the discrete digital signals, $f(t)$ and $g(t)$, have a length of N, the element length of output, $r(\tau)$, is $2N$–1, and the 0th lag is located in the middle of $r(\tau)$. Thus, only the second half of $r(\tau)$, starting at the 0th lag, was taken for the next processes.

Since the value of acoustic impedance must always be positive, but $r(\tau)$ has positive and negative fluctuations, we simply looked at the positive half of $r(\tau)$ by folding the record at mid-level. This can be done by taking the absolute values of $r(\tau)$.

The oscillating nature of $r(\tau)$ is caused by the fact that the two signals $f(t)$ and $g(t+\tau)$ are also oscillating at the central frequency (f_c=500 kHz in this study). When the two signals match the best, $r(\tau)$ would be the maximum. When these two signals are just off by half wavelength, $r(\tau)$ will become negative, but it will become a small positive number again when the lag approaches one wavelength. For this reason, it is understood that the high-frequency oscillating nature is not indicative of the fast change of correlation. Indeed, the envelope of $r(\tau)$ represents the change of correlation. Therefore, the above statements can be written as

$$\frac{\mathrm{d}Z(t)}{\mathrm{d}t} \propto E[|r(t)|] \tag{5}$$

where Z is the acoustic impedance, E the envelope, and $|r(t)|$ the processed signals after cross-correlation. Spikes of this envelope curve indicate the locations of the water–sediment interface and underlying substrata interface(s). The resolution of the measurement is also determined by the frequency of $g(t)$. Since 500-kHz supersonic waves have a wavelength of 3 mm, this would be the vertical resolution.

By integrating the gradient of acoustic impedance with time, a time series of acoustic impedance, $Z(\tau)$, can be calculated by

$$Z(\tau) = \rho_b(\tau)c = \int_0^\tau \frac{\mathrm{d}Z(t)}{\mathrm{d}t}\mathrm{d}t \tag{6}$$

where τ is the elapsed time, ρ_b the bulk density, and c the speed of sound in the medium.

Using $\tau=2z/c$, the signal of acoustic impedance in the time domain, $Z(\tau)$, can be converted into the acoustic impedance in the spatial domain, $Z(z)$. Since the speed of sound in water is almost the same as that in clay (Maa et al. 1997; also see the results of the present study below), variations in acoustic impedance can reasonably be attributed to variations in bulk density.

Because the processed acoustic echo strength cannot directly provide a value of bulk density, the signal needs calibration with ground-truth data in the post-processing stage. Details, including an example, are described below.

In another approach, the bulk density at the water–sediment interface can be explicitly estimated by Fresnel's reflection law,

$$R = \frac{\rho_2 c_2 - \rho_1 c_1}{\rho_2 c_2 + \rho_1 c_1} \tag{7}$$

where ρ is the density, c the speed of sound, and the subscripts 1 and 2 refer to the overlying water and the sediment layer, respectively. By rearranging Eq. 3, R can be estimated by

$$R(\theta, z, t) = \frac{2z\,P(z,t)}{P_0\sqrt{B(\theta)}} e^{2\alpha z} \tag{8}$$

Since all the parameters on the right-hand side of Eq. 8 are known, the reflection coefficient R for the water–sediment interface at the different geo-times can be determined. This is a simple and promising technique for estimating the bulk density of a near-bed layer without having to depend on an empirical relationship (Holland 2003). It is noted that the Fresnel's reflection method provides density estimates at the water—sediment interface, whereas the proposed empirical method provides density estimates in deeper sediment layers.

Results

Sample analysis

In tandem with acoustic measurements, the locations of water–sediment interfaces for the various consolidation stages were visually observed through the tank wall (see arrows in Fig. 4). As time elapsed, the water–sediment interface gradually migrated downward, while the suspended sediment concentration (or bulk density) below that interface gradually increased (Fig. 4). At an elapsed time of 1,034 h, the bulk density at 0.1 m above the tank bottom increased to about 1.25 g cm^{-3}. On the basis of the settlement rate of the interface level, the settling and consolidation states can be subdivided into three stages (Fig. 5):

1. During the first few hours, the water–sediment interface could not be determined because either there was no clear water–sediment interface, or the impedance difference was too small to be detected. At an elapsed time of 5 h, a first sharply defined interface was identified at 1.13 m, which subsequently dropped rapidly to 0.44 m by 24 h, leaving the overlying water relatively clear. During this stage, the settlement rate of the interface was approx. 3.6 cm h^{-1}.
2. Between 24 and 400 h, settling and consolidation continued at a moderate rate of approx. 0.06 cm h^{-1}, the interface being located at 0.22 m at the end of this stage.
3. After about 400 h, consolidation proceeded at a much lower rate, the interface being located at 0.2 m at the end of the experiment.

The consolidation state can also be determined from the reflection coefficient of the acoustic wave. This is dealt with below.

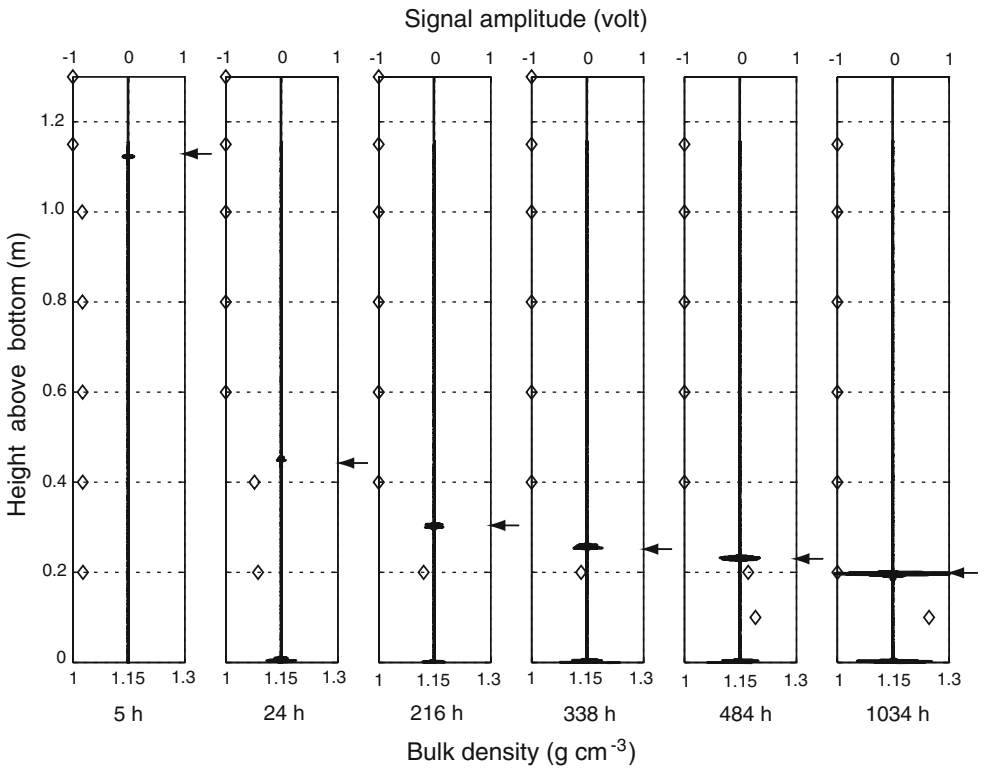

Fig. 4 Acoustic signals (*solid line* in each subplot) at various consolidation stages. *Diamonds* Bulk densities calculated from withdrawn samples, *arrows* locations of water–sediment interfaces visually observed through the tank wall

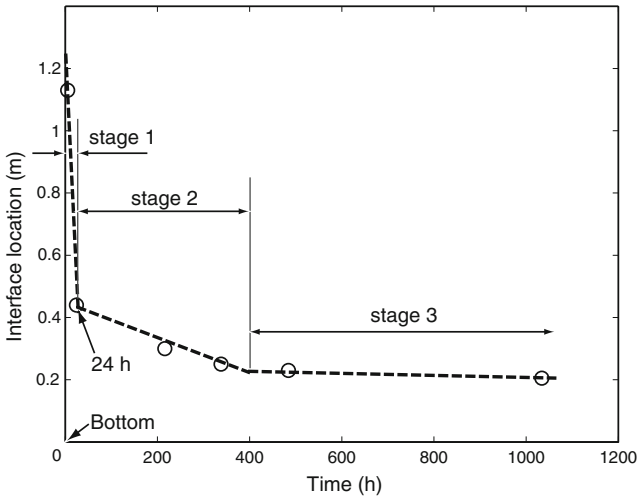

Fig. 5 Three stages of settling and consolidation based on the settlement rate of the water–sediment interface

Acoustic signal analysis

Due to the significant differences in acoustic impedance between clear water and sediment suspensions, the first salient peak in the return wave train was always encountered at the water–sediment interface, which was well correlated with the visually observed interface (Fig. 4). The echo signal strength from the first acoustic interface then progressively increased with consolidation time. Thus, the 5-h data show a relatively weak signal at the first peak. This can be explained in two possible ways. First, it may be caused by a weak density gradient near the water–sediment interface, because during the early stages of consolidation the bulk density gradient near the interface was not sufficiently large to generate a strong signal. Based on the sample-derived bulk densities, the bulk density gradient should be larger than about 0.025 g cm^{-3} for the present system to clearly detect the interface. A second reason may be related to the beam pattern of the source transducer used in the experiment. After 5 h, the distance between the source transducer and the water–sediment interface was about 0.17 m. Considering that the horizontal distance between the source and the receiver was only 0.05 m, the angle of reflection should be approx. 8.4° [=tan^{-1}(0.025/0.17)] in order to sense the return signal within the main lobe of the receiver. However, the employed source transducer had a beam angle of 4.6°. This indicates that the acoustic waves reflected from the water–sediment interface at 5 h were outside the main beam. As the water–sediment interface descended further with elapsed time, the return signal from the water–sediment interface gradually moved into the main beam. The effect of the beam angle eventually disappeared when the location of the water–sediment interface reached a distance of about 0.62 m below the transducer.

The second spike commonly occurred at the tank bottom, except for the 5-h data. At that time, the signal reflected from the tank bottom was too weak to be detected. This implies that the acoustic waves were mostly attenuated while traveling through the high-concentration (ca. 40 g l^{-1}) sediment-laden layer having a thickness of 1.13 m.

Signals backscattered by suspended particles are almost zero (see Fig. 4), showing very flat signals before reaching the water–sediment interface. This is because the wavelength (2–5 mm) of the Chirp signal is much longer than the diameter (≈1 μm) of the kaolinite particles, which explains the very low acoustic sensitivity (Ha et al. 2009). For this reason, the signals originating from the water column were not included in the calibration. Instead, the sample-derived bulk densities from below the water–sediment interface were compared with the processed signal (i.e., the signal output after the domain change shown in Fig. 3) strengths at the corresponding sampling levels (Fig. 6). The processed signal strength generally exhibits an exponential relationship with the true bulk density, leading to the following calibration equation:

$$\rho_b(z) = a + be^{kS(z)} \tag{9}$$

where a, b, and k are empirical coefficients calculated by using least-squares curve fitting, and $S(z)$ is the processed signal strength. It was assumed that ρ_b is 1 g cm^{-3} at S=0, representing a clear water condition.

While converting the processed signal strength in the time domain to the bulk density in the space domain, local speeds of sound had to be determined in both the water column and the consolidating mud layer. The two-way travel time (TWTT) between the transducer and the water–sediment interface (i.e., the first arrival peak in the envelope curve), and the corresponding propagation length were used

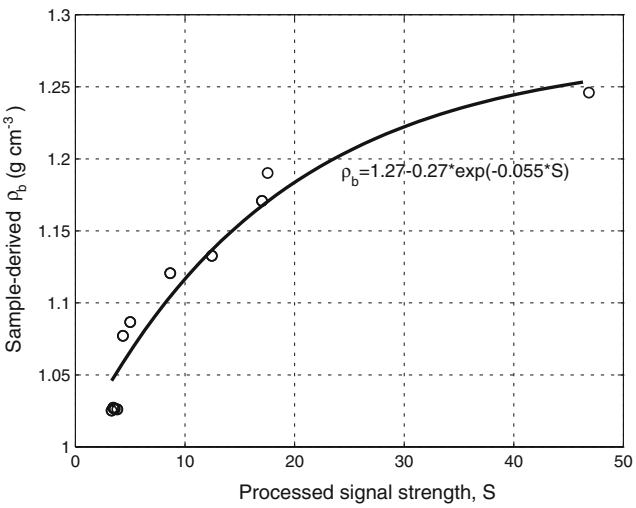

Fig. 6 Relationship between processed signal strength and sample-derived bulk density

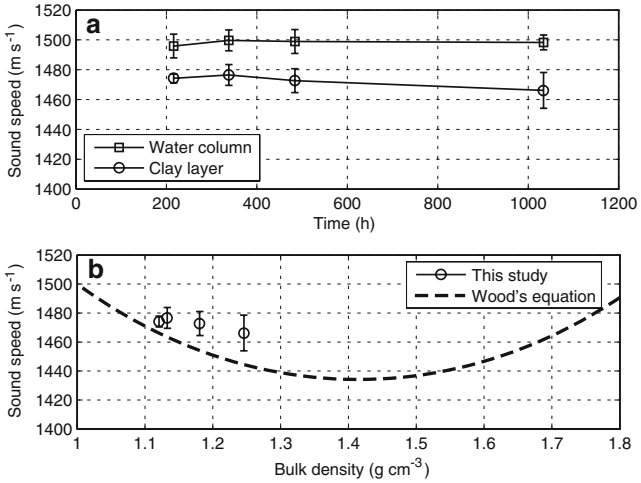

Fig. 7 **a** Sound speeds in the consolidating clay bed and the overlying water, and **b** sound speed versus bulk density in the consolidating clay bed. *Dashed line* Sound speed predicted by Wood's (1964) equation, *error bars* measured range

to determine the speed of sound in the water column. Similarly, the TWTT between the water–sediment interface and the tank bottom (i.e., the time interval between the first and the second arrival peak), and the visually observed sediment thickness were used to compute the speed of sound in the consolidating clay layer. Because a small amount of sediment was still suspended in the water column during the earlier stages (e.g., 5 and 24 h), only the data between 216 and 1,034 h were analyzed in order to strictly avoid any sound attenuation effect (even if insignificant in principle).

Figure 7a shows that the speed of sound in the consolidating clay bed was always slightly lower than that in the overlying water. On average, the speed of sound in the water column remained approx. 1,497 m s^{-1}. In the consolidating clay bed, by contrast, the average speed of sound showed a slight decreasing trend after 338 h; nevertheless, the rate of change was negligibly small considering the error ranges. The maximum speed of sound (1,499.6 m s^{-1}) in the water was only 2.3% higher than the minimum value (1,466.2 m s^{-1}) in the consolidating clay bed. It is therefore quite acceptable to use a single speed of sound value to convert the time series of signals to the space domain.

In order to verify the calculated speed of sound, the formula of Wood (1964) for estimating the speed of sound in clay beds with different bulk densities was used:

$$c = \left(\frac{1}{[\varphi/K_{\mathrm{w}} + (1-\varphi)/K_{\mathrm{s}}]\rho_{\mathrm{b}}} \right)^{1/2} \qquad (10)$$

where φ is the fractional porosity, and K_{w} and K_{s} are the bulk moduli of water and sediment, respectively. In Eq. 10, it is assumed that the rigidity introduced by the grain-to-grain contact was negligible. However, it was found that the speeds of sound in the consolidating clay beds were actually slightly higher than those predicted by Wood's equation (Fig. 7b). In this context, Jackson and Richardson (2007) pointed out that higher measured values are related to the presence of rigidity in the consolidating bed, a fact not considered in Eq. 10, as pointed out above.

Reflection coefficient and bulk density

The predetermined speeds of sound and R are required to calculate the bulk density. Due to the previously described limitations in beam geometry for this experiment, R and bulk density were estimated only between 216 and 1,034 h. Both R and bulk density gradually intensified with the consolidation time. At the end of the measurement series, R had increased to 0.118, and the bulk density to 1.29 g cm^{-3} (Fig. 8). The difference between bulk densities estimated both with and without the measured sound speed in clay was about 1–2%, which is also practically negligible (Table 1). The estimates of bulk density at the water–sediment interface should be less than or nearly equal to the average bulk density of the sediment layer. All estimates based on Fresnel's reflection equation showed slightly less than the average of the bulk density in the sediment layer, except the 1,034-h data, which might be due to errors in measurement (Figs. 4 and 8). As the difference in bulk density between the clay layer and the overlying water became larger with time, the difference in acoustic impedance increased accordingly. This increase, which suggests that consolidation in the surface layer was still in progress even after 1,034 h, was plausibly caused by consolidation-induced factors (e.g., dewatering, decrease in porosity, and increase in bed rigidity). Consequently, the

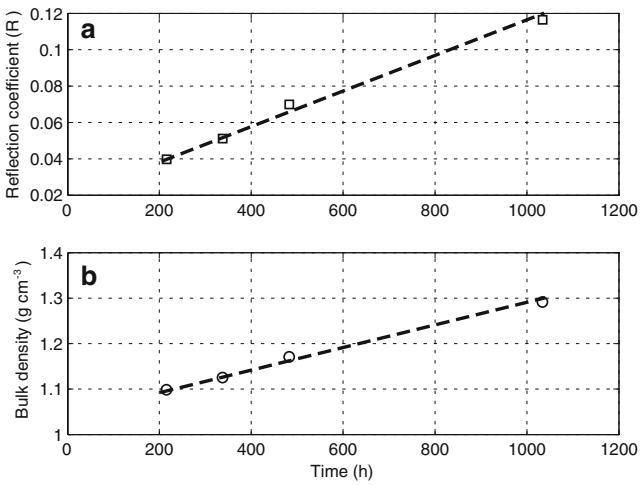

Fig. 8 Temporal evolution of the acoustic wave reflection coefficient (**a**), and the bulk density (**b**) at the water–sediment interface during consolidation. *Dashed lines* Best-fit linear regressions

Table 1 Comparison of bulk densities estimated by three different methods

Elapsed time (h)	Bulk density (g cm^{-3})		
	Water sample	Micro-Chirp	Fresnel equation
216	1.1207	1.1045	1.0987 (1.0827)[a]
338	1.1328	1.1366	1.1252 (1.1079)
484	1.1806	1.1704	1.1710 (1.1504)
1,034	1.2459	1.2539	1.2913 (1.2636)

[a] Values in parentheses were estimated by assuming that the sound speed in clay is equal to that in water

bulk density and the maturity of consolidation state in the surface layer can be acoustically gauged by measuring changes in R.

Discussion

Possible limitations

Despite the advantages of the Micro-Chirp acoustic system over other methods, it still has room for improvement. In Eq. 5, the envelope curve is claimed to be proportional to the gradient of acoustic impedance. Since the envelope curve always shows a positive value, there is no possibility for impedance or bulk density to decrease. In estimating the vertical profile of bulk density in sediment layers, this is a weakness of this developed signal-processing protocol. It is noted, however, that the main target of this study is to quickly estimate the average bulk density in the top (approx. a few centimeters) clay layer. In order to provide the deeper profile of bulk density, therefore, the penetration depth of the Micro-Chirp acoustic system must be extended by employing a high-power amplifier and related instruments, and the sound attenuation in the sediment layer should be also taken into account. Further validation involving the signal-processing algorithm should be done.

Future field application

In order to deploy the developed Micro-Chirp acoustic system in the field, some hardware modifications will be necessary even though most of the instrumentation would normally be found on board a ship. Thus, a firm underwater mounting frame will be needed to hold the transducers. Unlike the laboratory setup, the location and alignment of transducers in the field are more critical to avoid negative influences on the return signal strength and the grazing angle of the transmitted beam, because turbulence will continuously exert mechanical forces to the underwater units. It is therefore recommended that motion sensors that detect tilting angles and depth be installed in order to correctly compensate the sound reflection and spreading loss caused by the motion of the underwater units.

At deeper deployment sites, more attenuation and spreading of return signals should be taken into account, because the return acoustic waves would be significantly dampened by the water and suspended materials. Sound attenuation, in particular, is extremely high if a high-concentration layer such as a fluid mud is formed near the bed. In addition, signal contamination while traveling along the connecting cable between the onboard units and the underwater units is inevitable. To effectively boost the attenuated return signals, the linear signal conditioner used in this laboratory study should be replaced by a logarithmic (>80 dB) signal conditioner that is capable of amplifying the true return signal more powerfully than the background noise. It is preferable that this amplifier and ADC unit be enclosed in a watertight container to be mounted in the frame as close as possible to the receiving transducer.

In muddy environments, the developed signal-processing protocol can conveniently be used to estimate the consolidation state and bulk density. If the bottom sediment is composed of either sand or heterogeneous mixtures of sand and mud, the correct determination of the speed of sound in the sediment bed is critical for accurate bulk density measurements. This is because the precision in the speed of sound is a main parameter to determine the vertical resolution of bulk density. The speed of sound in pure mud is ca. 1,450 m s^{-1}, whereas in pure sand it is ca. 1,750 m s^{-1} (Maa and Lee 2002). Further investigations are therefore needed to develop a new algorithm that considers variations in the speed of sound for various mixtures of sand and mud. Incorporation of a sound velocimeter in the instrument package may partly solve this problem. In addition, a number of independent, site-specific bulk density measurements should be carried out to have reference values for calibration purposes (e.g., Flemming and Delafontaine 2000; Tolhurst et al. 2005).

Conclusions

The main conclusions drawn from this study are:

1. The measured acoustic responses demonstrate that settling and consolidation of suspended mud resulted in progressively increasing bulk densities of the

sediment bed, and differences in acoustic impedance near the water–sediment interface. Accordingly, the acoustic wave reflectivity at that interface increased with consolidation time. Because the speed of sound in the clay bed hardly changed, and its value is close to that of water, a single velocity of sound value can be used for practical bulk density estimations in muddy environments.

2. The developed Micro-Chirp acoustic system and its signal-processing protocol yield remote estimations of bulk density and consolidation state in consolidating clay beds. This technique can be applied for in-situ bulk density measurements within the top layer of a sediment bed after proper system calibration by means of in-situ sediment samples.

Acknowledgements This study was partly supported by a VIMS graduate research grant, and the final preparation of manuscript was done at KOPRI. This paper benefited from the critical review of an anonymous referee, and useful suggestions from the journal editors.

References

Been K, Sills G (1981) Self-weight consolidation of soft soils: an experimental and theoretical study. Géotechnique 31(4):519–535

Briggs KB, Richardson MD (1996) Variability in in situ shear strength of gassy muds. Geo-Mar Lett 16(3):189–195. doi:10.1007/BF01204508

de Groot AV, van der Graaf ER, de Meijer RJ, Maučec M (2009) Sensitivity of in situ γ-ray spectra to soil density and water content. Nucl Instrum Methods Phys Res A 600:519–523

Dowling JJ (1990) Estimating porosity of partially saturated sediment. Eng Geol 29:139–147

Flemming BW (2002) Geographic distribution of muddy coasts. In: Healy TR, Wang Y, Healy J-A (eds) Muddy coasts of the world: processes, deposits, and function. Elsevier, Amsterdam, pp 99–201

Flemming BW, Delafontaine MT (2000) Mass physical properties of muddy intertidal sediments: some applications, misapplications, and non-applications. Cont Shelf Res 20:1179–1197

Fontein W, van der Wal J (2006) Assessing nautical depth efficiently in terms of rheological characteristics. In: Evolutions in Hydrography. Proc Int Hydrographic Conf Hyrdo'06, 6–9 November 2006, Antwerp, Belgium. Spec Publ Hydrogr Soc 55:149–152

Ha HK, Hsu W-Y, Maa JP-Y, Shao Y, Holland CW (2009) Using ADV backscatter strength for measuring suspended cohesive sediment concentrations. Cont Shelf Res 29:1310–1316

Hamilton EL (1971) Elastic properties of marine sediments. J Geophys Res 76:579–604

Hawley N (1981) Mud consolidation during a short time interval. Geo-Mar Lett 1(1):7–10. doi:10.1007/BF02463294

Hirst TJ, Rerlow M, Richards AF (1975) Improved in situ gamma-ray transmission densitometer for marine sediments. Ocean Eng 3:17–27

Holland CW (2003) Seabed reflection measurement uncertainty. J Acoust Soc Am 114(4):1861–1873

Holland CW, Dettmer J, Dosso SE (2005) Remote sensing of sediment density and velocity gradients. J Acoust Soc Am 118(1):163–177

Jackson DR, Richardson MD (2007) High-frequency seafloor acoustics. Underwater Acoustics Series. Springer, New York

Jacob W, Eelkema M, Limburg H, Winterwerp JC (2009) A new radiometric instrument for in situ measurements of physical sediment properties. Mar Freshw Res 60:727–736

Kaya A, Yoshida H, Tanigawa H, Igata H, Tsuruya H (2008) Estimation of sea bottom density profile through analysis of ultrasonic echo signals. In: Kusuda T, Yamanishi H, Spearman J, Gailani JZ (eds) Sediment and ecohydraulics: intercoh 2005. Elsevier, Amsterdam, pp 17–30

LeBlanc LR, Mayer L, Rufino M, Schock SG, King J (1992) Marine sediment classification using the chirp sonar. J Acoust Soc Am 91(1):107–115

Libicki C, Bedford KW (1989) Remote and in situ methods for sub-bottom sediment characterization. J Coast Res 5:39–49

Lintern DG, Sills GC, Feates N, Roberts W (2002) Erosion properties of mud beds deposited in laboratory settling columns. In: Winterwerp JC, Kranenburg C (eds) Fine-sediment dynamics in the marine environment. Elsevier, Amsterdam, pp 343–357

Maa JP-Y, Lee D-Y (2002) A preliminary study on using acoustic waves to measure high resolution marine sediment bed structure. In: Winterwerp JC, Kranenburg C (eds) Fine-sediment dynamics in the marine environment. Elsevier, Amsterdam, pp 469–481

Maa JP-Y, Sun K-J, He Q (1997) Ultrasonic characterization of marine sediments: a preliminary study. Mar Geol 141:183–192

Mehta AJ, Dyer KR (1990) Cohesive sediment transport in estuarine and coastal waters. In: LeMehaute B, Hanes DM (eds) The sea: ocean engineering science. vol 9, part B. Wiley, New York, pp 815–839

Mole LA, Hunter JL, Davenport JM (1972) Scattering of sound by air bubbles in water. J Acoust Soc Am 52:837–842

Partheniades E (2006) Engineering properties and hydraulic behavior of cohesive sediments. CRC Press, Boca Raton

Schrottke K, Becker M, Bartholomä A, Flemming BW, Hebbeln D (2006) Fluid mud dynamics in the Weser estuary turbidity zone tracked by high-resolution side-scan sonar and parametric sub-bottom profiler. In: Bartholomä A, Winter C (eds) Coastal dynamics and human impact: south-eastern North Sea. Geo-Mar Lett 26(3):185–198. doi:10.1007/s00367-006-0027-1

Seifert A, Stegmann S, Mörz T, Lange M, Wever T, Kopf A (2008) In situ pore-pressure evolution during dynamic CPT measurements in soft sediments of the western Baltic Sea. Geo-Mar Lett 28 (4):213–227. doi:10.1007/s00367-008-0102-x

Sills GC (1997) Consolidation of cohesive sediments in settling columns. In: Burt N, Parker R, Watts J (eds) Cohesive sediments. Wiley, New York, pp 107–120

Sills GC (1998) Development of structure in sedimenting soils. Philos Trans R Soc Lond 356:2515–2534

Skaropoulos NC, Yagridou HD, Chrissoulidis DP (2003) Interactive resonant scattering by a cluster of air bubbles in water. J Acoust Soc Am 113(6):3001–3011

Stark N, Wever TF (2009) Unraveling subtle details of expendable *b*ottom *p*enetrometer (XBP) deceleration profiles. Geo-Mar Lett 29(1):39–45. doi:10.1007/s00367-008-0119-1

Stearns SD (2003) Digital signal processing with examples in Matlab. CRC Press, Boca Raton

Tolhurst TJ, Underwood AJ, Perkins RG, Chapman MG (2005) Content versus concentration: effects of units on measuring the biogeochemical properties of soft sediments. Estuar Coast Shelf Sci 63:665–673

Torfs H, Mitchener H, Huysentruyt H, Toorman E (1996) Settling and consolidation of mud/sand mixtures. Coast Eng 29:27–45

Verbeek H, Cornelisse J (1995) Consolidation of dredged sludge, measured by an acoustic densitometer. Mar Freshw Res 46:179–188

Winterwerp JC, van Kesteren WGM (2004) Introduction to the physics of cohesive sediment in the marine environment. Elsevier, Amsterdam

Wood AB (1964) A textbook of sound. Bell G, London